

# HNPS Advances in Nuclear Physics

Vol 30 (2024)

HNPS2023



## Radioactivity mapping of beach sand by mobile in situ gamma-ray spectrometry

*Dionysios Patiris, Christos Tsabaris, Christos Maramathas, Stylianos Alexakis, Spyridoula Konstantina Roumelioti*

doi: [10.12681/hnpsanp.6269](https://doi.org/10.12681/hnpsanp.6269)

Copyright © 2024, Dionysios Patiris, Christos Tsabaris, Christos Maramathas, Stylianos Alexakis, Spyridoula Konstantina Roumelioti



This work is licensed under a [Creative Commons Attribution-NonCommercial-NoDerivatives 4.0](https://creativecommons.org/licenses/by-nc-nd/4.0/).

### To cite this article:

Patiris, D., Tsabaris, C., Maramathas, C., Alexakis, S., & Roumelioti, S. K. (2024). Radioactivity mapping of beach sand by mobile in situ gamma-ray spectrometry. *HNPS Advances in Nuclear Physics*, 30, 116–123. <https://doi.org/10.12681/hnpsanp.6269>

# Radioactivity mapping of beach sand by mobile in situ gamma-ray spectrometry

D. Patiris<sup>1,\*</sup>, C. Tsabaris<sup>1</sup>, C. Maramathas<sup>2</sup>, S. Alexakis<sup>1</sup>, S.K. Roumelioti<sup>2,3</sup>

<sup>1</sup> *Institute of Oceanography, Hellenic Centre for Marine Research*

<sup>2</sup> *teleDOS Laboratories S.M. P.C., 20131, Corinth, Greece*

<sup>3</sup> *Department of Physics, National Technical University of Athens*

---

**Abstract** A new method for prompt radioactivity mapping of beach sand is under development. It is based on mobile in situ gamma-ray spectrometry exploiting low- and medium-resolution portable scintillator systems. Two case study applications are presented which took place during IAEA's RER1020 and CRP F22074 projects, aiming to determine the main methodological features, capabilities, and limitations of the new method. In general, spectra of very short acquisition time (20s) are obtained by a mobile unit (man or vehicle) along transects on the beach sand. The statistic of each spectrum is extremely low for individual analysis; however, the spatial resolution of each measurement is preserved high (a few meters). The distribution of the total counting rate is used to classify the spectra, according to quartiles, into four classes (high, low, medium-high, and medium-low). For each class, the spectra are combined into one of a total acquisition time high enough for spectrometric analyses. Laboratory HPGc measurements and simulation studies were used to calculate the efficiency of selected photo-peak energies. The first maps obtained by the mobile method are in very good agreement with those obtained by grid sampling and laboratory analyses. Critical aspects under further investigation regard the varied physical parameters of the beach sand (density, water content, porosity) and the complicated detection geometry both of them strongly related to the detection efficiency.

**Keywords** In-situ gamma-ray spectrometry, Coastal area radioactivity mapping, Marine radioactivity, Sediment dynamics, Radio-tracing.

---

## INTRODUCTION

During the last decades, coastal areas have significant socioeconomic impact on their population. Anthropogenic activities related to industrial and mining activities, energy production and touristic development significantly stress coastal areas resulting in pollution, degradation and erosion effects. Radioactivity monitoring and mapping of coastal areas reveals their radioecological status [1]–[3] but also, according to recent studies [4]–[8], may indicate sediment dynamics processes such as erosion and accretion. The radionuclides of radium  $^{226}\text{Ra}$  and  $^{228}\text{Ra}$  are progenies of  $^{238}\text{U}$  and  $^{234}\text{Th}$  natural radioactive series respectively. Both are present in the crystal structure of minerals with  $^{228}\text{Ra}$  being mostly related to weaker bound carbonate salts. As a result, minerals rich in  $^{228}\text{Ra}$  carbonates can be more easily eroded than those of  $^{226}\text{Ra}$  providing a radio-tracing technique when the ratio  $^{226}\text{Ra}/^{228}\text{Ra}$  can be estimated. Where the ratio is higher erosion processes are predominant while lower values of the ratio indicate accretion of eroded sediment rich in  $^{228}\text{Ra}$ .

In most published radioactivity mapping applications in coastal areas, sampling of beach sand sediment on a topographic grid takes place followed by sample preparation and radioactivity measurement with laboratory equipment. That approach is time-consuming and demands prolonged laboratory processes, consumables and manpower. On the other hand, the in situ dosimeter technique although quick and prompt, lacks the capacity for specified radionuclides detection. Thus, this work aims to develop a new method for prompt, real-time radioactivity mapping of a coastal area based on mobile in-situ gamma-ray spectrometry. The advantages of the mobile in-situ approach are the rapidness and cost efficiency, the extended spatial coverage and hot-spot localization. However, as it is

---

\* Corresponding author: [dpatiris@hcmr.gr](mailto:dpatiris@hcmr.gr)

based on low to medium-resolution scintillation detection systems, the identification of radionuclides is restricted due to the convolution of photo-peaks and spectrum shift due to temperature variation should be tackled. Also, intended to be a rapid method causes measurements of higher uncertainty as acquisition time is significantly lower than that of the laboratory methods. However, despite the weaknesses, during the last decade mobile in situ gamma-ray spectrometry has been exploited in a wide range of environmental radioactivity studies [9–16] providing spatial and temporal data in real, and sometimes harsh, environmental conditions. In the present work, the proposed method was applied at a coastal area of the south Attica region during 2021 and 2023 fieldwork campaigns of IAEA projects to rapidly estimate natural radionuclides activity levels of the beach sand and reveal any trend of their spatial distribution.

## EXPERIMENTAL DETAILS

### *Mobile in situ gamma-ray spectrometry implementation*

The low-resolution, NaI(Tl) crystal-based, underwater gamma-ray spectrometer KATERINA II was used, mounted on a backpack for person carriage. The detector was synchronized with a GPS receiver, a data communication and recording system while the whole acquisition was guided by a small portable Raspberry microcomputer. In Figure 1 a schematic depiction of the method implementation is presented. A person carried the backpack walking almost constantly on the beach sand with an approximate velocity of  $4 \text{ km h}^{-1}$ . The detector's crystal was about 1 m above the beach sand and set to continual loop operation with an acquisition time for each spectrum equal to 20 s. Thus, a sequence of spectra was acquired each one related with a walking distance of about 20 m. The GPS receiver recorded the position of the detector every 10 s so the start, middle and final point of each 20 m interval were logged. Taking the middle point for each interval as a position reference, a mobile grid is created. Each point of it is corresponded with a spectrum of 20 s. The Total Counting Rate (TCR) is the average per second number of all detected gamma-rays and it is rapidly calculated for each spectrum. The user can observe in real-time TCR values and variations and accordingly can re-orient the walking route. That feature makes possible a “hot spot” localization and in general provides the user the capability to acquire more spectra in areas of interest.

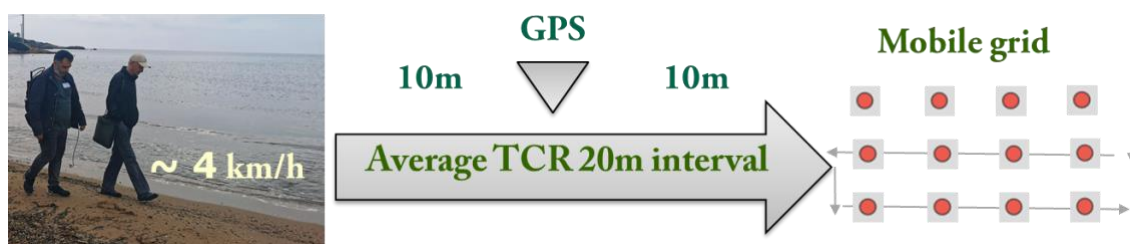


**Figure 1.** Schematic depiction of the mobile in situ gamma-ray spectrometry on beach sand. As the person who carries the system walks steadily, a grid of points is created each one corresponding to a spectrum.

### *Methodology description*

When using mobile in situ gamma-ray spectrometry, a database is generated which contains information about multiple grid positions, including their longitude and latitude and corresponding spectra. However, since the acquisition time for each spectrum is too short, it is not possible to perform individual full-spectrum analyses. Therefore, it is essential to have a methodology for grouping, summing, and analysing these spectra. The TCR values have been used for grouping them because their uncertainty is low even with the short 20s acquisition time. The methodology is separated and described in the following steps:

1. The acquired spectra are aggregated into four classes by dividing the distribution of TCR values into four quartiles. A quartile is a type of quantile that divides the number of TCR values into four parts of more or less equal size. Among the several division methods, the "Tukey's hinges" is used [17]. The median value divides the TCR data set into two halves, the lower and upper. Then, the two halves are again divided by the corresponding halves medians, the lower quartile value is the median of the lower half of the TCR values and the higher quartile is the median of the higher one. Thus, the spectra are grouped into four TCR classes of equal population named High, Medium High, Medium Low and Low.
2. For each TCR class, the individual spectra are combined into one spectrum by summing the number of counts channel by channel. The aggregate spectrum has a much longer acquisition time and can be used for full spectrum analyses.
3. Each TCR class spectrum is calibrated and photo-peak analyses take place for the radionuclides of interest to estimate their activity concentration.
4. For the radionuclides of interest, the activity concentration values are assigned to the grid points according to the TCR class each spectrum belongs.
5. Interpolation and mapping.

The entire methodology, including spectrum analyses, interpolation and map production, has been implemented using R-language code. R is a programming language used for statistical computing and graphics. It supports various statistical methods such as linear and nonlinear modelling, classical statistical tests, time-series analysis, classification, clustering, and many others. R is available as free Software under the terms of the Free Software Foundation's GNU General Public License and runs on a wide variety of UNIX platforms and similar systems Windows and MacOS.

#### *Full energy photo-peak efficiency*

The calculation of the activity concentration of the radionuclides of interest, demands the estimation of the corresponding full energy photo-peak efficiency (FEPE). FEPE is dependent on the gamma-ray energy and rather complicated methods have been developed to estimate it in different material matrices (e.g. seawater, fresh water and marine sediment) combining experimental and theoretical data obtained by MC simulation codes [18]–[21]. For that preliminary work, a simplified simulation model developed using the EGSnrc MC Simulation code [22] and an inter-calibration technique were used as the first methodological step of FEPE estimation regarding the radionuclides of the beach sand [23]. For the theoretical estimation, the effective volume is defined by a cylinder with a diameter of 3 m and a height of 0.3 m. From that volume, gamma-rays are emitted while the detector crystal is 1 m above the cylinder surrounded by air containing a negligible concentration of radionuclides. The simulation model was supported by experimental data. Samples were collected from two different positions. The sediment wet density was measured on-site, dry density was measured after drainage of 3d in the laboratory and the percentage of sediment's water content was estimated. From the same positions, 1 h stationary spectra were collected by the KATERINA II. The massive activity concentration of the radionuclides of interest was measured by HPGe and the results were used to inter-calibrate the in situ spectrometer regarding the FEPE of  $^{40}\text{K}$  (1460 keV),  $^{214}\text{Bi}$  (1720 keV) and  $^{208}\text{Tl}$  (2600 keV). The estimation is limited to the specific coastal area as a general model demands much more experimental and theoretical data involving different physical sediment parameters (density, water content, minerals constituent, etc.), effective volume and geometrical considerations.

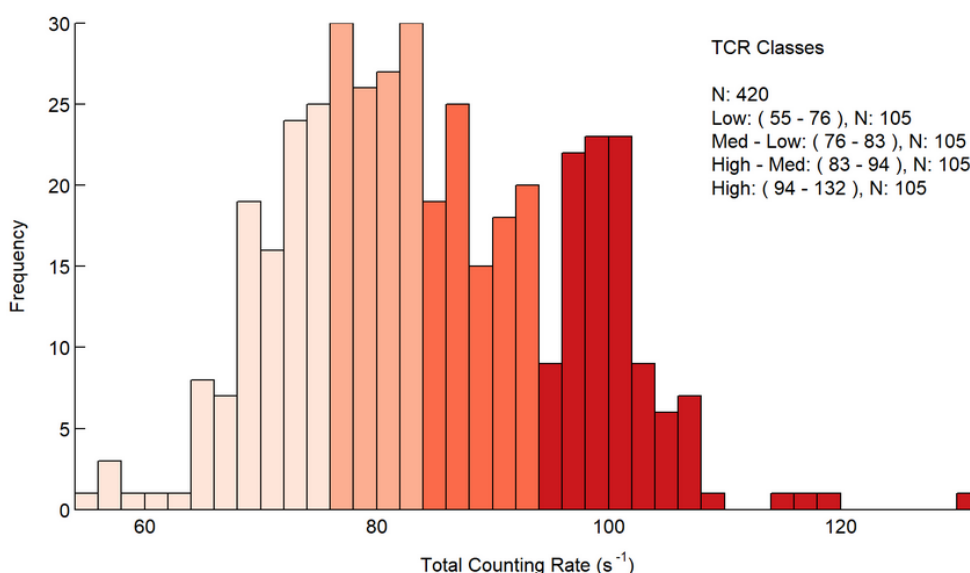
## **RESULTS AND DISCUSSION**

The results and maps obtained by the implementation of the proposed method in the coastal area of Limani Passa (southern Attica) during the 2021 and 2023 fieldwork campaigns are presented. In Fig.

2 the spatial distribution of TCR values is presented (2a) according to the four classes of TCR distribution (2b) as described in steps 1 and 2 mentioned in the methodology description section.



(a)



(b)

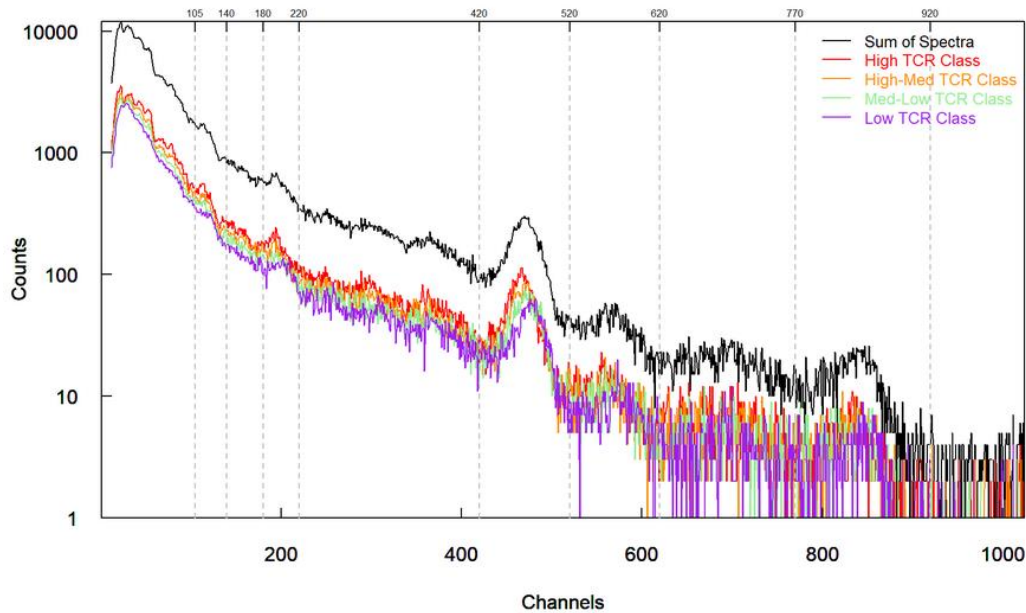
**Figure 2.** (a) TCR spatial distribution on the beach sand of L.Passa during the 2021 campaign, (b) TCR values distribution and the four classes according to TCR quartiles

The total number of the individual spectra was 420 so, each class contains 105 spectra of 20 s. For each class, one corresponding spectrum is created by summing their counts channel by channel. By combining the individual spectra this way, small drifts during the acquisition may result in broadening of the full width at half maximum of the observed photo-peaks. The combined spectra, as well as their sum, are presented in the Figure 3a as uncalibrated spectra to allow for easy observation of small drifts. The spectrum of each class is energy calibrated and the analyses of the photo-peaks of  $^{40}\text{K}$  (1460 keV),  $^{214}\text{Bi}$  (1720 keV) and  $^{208}\text{Tl}$  (2600 keV) take place for Compton background subtraction using a second-order polynomial regression model as depicted in the Figure 3b for the case of the sum of all individual spectra.

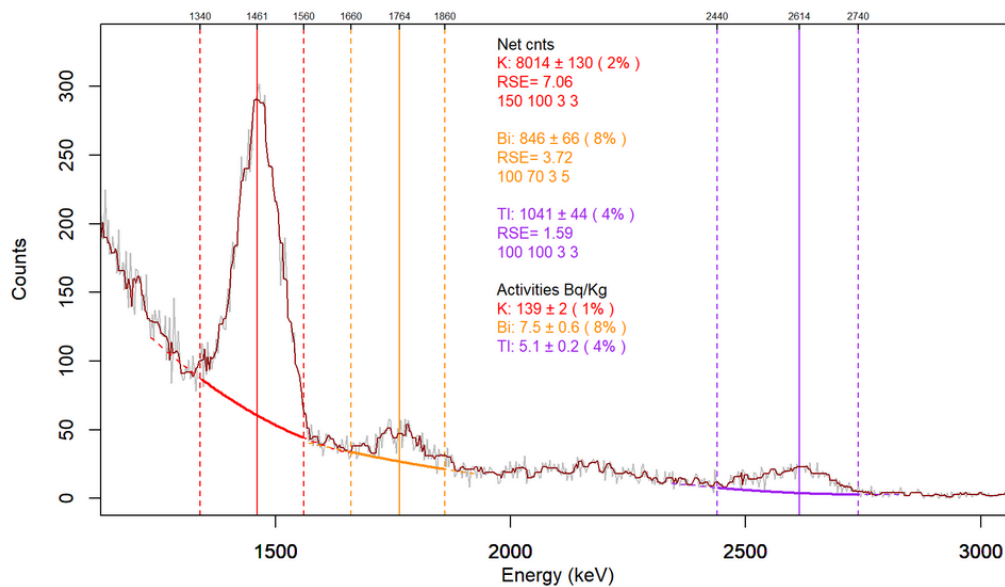
The per second net area counting rate (NetArea CR) of each photo-peak is converted to massive activity concentration (Act) using equation 1.

$$Act = \frac{\text{Net Area CR}}{FEPE \cdot I_g \cdot \pi r^2 h \cdot d_{dry}} \tag{1}$$

where  $FEPE$  is the full energy photo-peak efficiency,  $I_g$  is the branching ratio,  $d_{dry}$  is the density of the dried sediment sample, and  $r$  and  $h$  are the radius and height of the cylindrical effective volume. The massive activity concentration is presented in Table 1 for the sum of all spectra as well as for each TCR class spectrum.



(a)



(b)

**Figure 3.** (a) The spectra are created by summing channel by channel the individual spectra according to the TCR class. Also, the spectrum of the sum of all individual spectra is presented (black line). Slight drifts of the spectra are observed resulting in broader peaks of slightly higher FWHM. (b) Spectrum energy calibration ( $E > 1000$  keV) and photopeak analyses (Compton background subtraction) for the case of the spectrum which is the sum of all individual spectra.

It is important to note that the separation of TCR classes is a statistical method of combining individual spectra because of their short acquisition time. The TCR uncertainty is generally low, so the separation of TCR values into classes is usually statistically significant. However, if the activity concentration of a radionuclide significantly varies from class to class, it should always be considered along with the measured uncertainties. This means that if the spatial distribution of one or more radionuclides is almost constant, the different classes may not have any physical meaning. In the case of Limani Passa, the activity concentration of  $^{40}\text{K}$  varied significantly according to TCR classes when accounting for measured uncertainties. In contrast, the  $^{208}\text{Tl}$  activity concentration variation was not statistically significant, indicating an almost constant spatial distribution. The activity concentration of  $^{214}\text{Bi}$  in high and low TCR classes varied significantly from each other, while their variation from the intermediate TCR classes cannot be considered significant.

**Table 1.** Massive activity concentration of the radionuclides of interest

TCR Class	$^{40}\text{K}$ 1461 keV Bq kg <sup>-1</sup>	$^{214}\text{Bi}$ 1764 keV Bq kg <sup>-1</sup>	$^{208}\text{Tl}$ 2640 keV Bq kg <sup>-1</sup>
<b>Sum</b>	139 ± 2	7.5 ± 0.6	5.1 ± 0.2
<b>High</b>	193 ± 5	9.7 ± 1.0	5.5 ± 0.5
<b>High Med.</b>	148 ± 5	8.1 ± 1.0	4.7 ± 0.4
<b>Med. Low</b>	135 ± 4	7.6 ± 1.0	5.2 ± 0.4
<b>Low</b>	101 ± 4	6.6 ± 1.0	4.9 ± 0.4

The activity concentration value of each radionuclide is allocated to the acquisition grid point and the Inverse Distance Weighting (IDW) method is used to estimate the spatial distribution of the activity concentration to the whole area of the beach by interpolation. IDW interpolation is a mathematical (deterministic) method assuming that closer values have a higher impact on a point than values at a greater distance. Although, it is a commonly used method for spatial statistical analyses, should be used carefully in case of outliers (e.g. existence of “point sources”). As an example in Figure 4, the allocation of the activity concentration of  $^{214}\text{Bi}$  to the grid points (4a) and the map produced by interpolating the experimental values (4b) are depicted.

As already referred, the extent to which a variation of the activity concentration values is statistically significant or not should be considered by the measured uncertainty. The use of interpolation maps is however a convenient tool to indicate spatial trends and potential radiological areas of interest. The interpolation results were also used to investigate trends of radionuclides' activity concentration ratios. The ratio of  $^{214}\text{Bi}/^{208}\text{Tl}$  (equivalent to  $^{226}\text{Ra}/^{228}\text{Ra}$  due to radioactive equilibrium) was calculated and the values are presented in an interpolation map to indicate areas of beach erosion. According to the referred literature, higher ratio values (“rich” in  $^{226}\text{Ra}$ ) indicate erosion of the beach while lower values (“rich” in  $^{228}\text{Ra}$ ) indicate areas of sediment accretion.

The case of Limani Passa beach is typical of a natural erosion process. Rainwater flowing toward the sea, via water paths and small streams easily observed on the map, erodes the terrestrial part of the beach. The eroded material is moved to the sea and taking part in sediment transportation processes, is finally accumulated at the beachfront.



(a)



(b)

**Figure 4.** (a) The spatial distribution of  $^{214}\text{Bi}$  massive activity concentration ( $\text{Bq kg}^{-1}$ ) and (b) the respective map as produced by IDW interpolation method during the 2021 fieldwork campaign.

In Figure 5, the interpolation mapping of the ratio is depicted as obtained during the two fieldwork campaigns in 2021 (5a) and 2023 (5b). During both periods, higher ratio values can be observed at the northern area of the beach while lower values at the southern area which is closer to seawater.



(a)



(b)

**Figure 5.** The spatial distribution of  $^{214}\text{Bi}/^{208}\text{Tl}$  ratio (equivalent to  $^{226}\text{Ra}/^{228}\text{Ra}$  due to radioactive equilibrium) indicates areas of beach erosion (higher values) and sediment accretion and accumulation (lower values) during the 2021 (a) and 2023 (b) fieldwork campaigns.

## CONCLUSIONS

The mobile in situ gamma-ray spectrometry method was implemented in a reference coastal area of southern Attica, specifically Limani Passa beach, during the 2021 and 2023 fieldwork campaign conducted as part of the IAEA Regional Workshop “Radiometric Methods for Sediment Dynamics Evaluation”. The method involved using a low-resolution gamma-ray spectrometer KATERINA II to provide spectra every 20 seconds during walking routes on the beach sediment. This approach was found to be effective in providing maps of natural radionuclide activity concentration values, as well as indicating areas of beach erosion and sediment accretion. These preliminary results are encouraging and support further investigation in developing a general method for efficiency (FEPE) calibration that takes into account the peculiarities of the beach sand material. Unlike soil or marine sediment which are mostly dry and wet respectively, beach sand can be dry at the surface and get moist to wet deeper in the sediment. This higher pore water content results in higher attenuation of gamma-rays in the sediment, which strongly affects the efficiency of the method (FEPE). Additionally, given that the sediment of a coastal area may have several terrestrial origins, different densities and mineral constituents may be encountered in beach sand, both of which can affect FEPE.

In conclusion, despite its drawbacks such as high uncertainty and low energy resolution, the method can rapidly and cost-effectively provide a first estimation of the spatial distribution of radionuclides of interest in coastal regions. It can be also used to direct and optimize sampling and monitoring activities of higher precision, accuracy, and cost.

## Acknowledgments

Supported by IAEA projects RER1020 “Radiometric Methods for Sediment Dynamics Evaluation” and CRP F22074, “Development of Radiometric Methods and modelling for measurement of sediment transport in coastal systems and rivers”.

## References

- [1] F.K. Pappa et al., Environ. Sci. Pollut. Res. 25, 30084 (2018)
- [2] F.K. Pappa et al., Environ. Sci. Pollut. Res. 26, 27457 (2019)
- [3] F.K. Pappa et al., Appl. Radiat. Isot. 145, 198 (2019)
- [4] J. Wang, J. Du, and Q. Bi, Mar. Pollut. Bull. 114, 602 (2017)
- [5] A.C. Arriola-Velásquez et al., Catena 235, no. February 2023 (2024)
- [6] A. Arriola-Velásquez et al., Estuar. Coast. Shelf Sci. 231, 106476 (2019)
- [7] J. Du et al., Reg. Stud. Mar. Sci. 48, 102061 (2021)
- [8] Z.J. Dai et al., Environ. Earth Sci. 62, 1629 (2011)
- [9] P. Kock, C. Rääf, and C. Samuelsson, J. Env. Rad. 128, 84 (2014)
- [10] A. Varley, A. Tyler, and C. Wilson, 223–224, 106400 (2020)
- [11] A. Varley et al., Environ. Pollut. 240, 191 (2018)
- [12] D.L. Patiris et al., Appl. Radiat. Isot. 140, 305 (2018)
- [13] J.P. Balbuena et al., NIM A 859, 1 (2017)
- [14] C. Lee, S.W. Park, and H.R. Kim, NIM A 966, 163833 (2020)
- [15] E. Prieto et al., Radiat. Phys. Chem. 168, 108600 (2020)
- [16] M.S. Lee et al., Nucl. Eng. Technol. 55, 2158 (2023)
- [17] Tukey, John Wilder (1977), Exploratory Data Analysis, ISBN 978-0-201-07616-5
- [18] G. Cinelli, L. Tositti, D. Mostacci, and J. Baré, J. Environ. Radioact. 155–156, 31 (2016)
- [19] E.G. Androulakaki et al., J. Environ. Radioact. 164, 47 (2016)
- [20] E.G. Androulakaki et al., Appl. Radiat. Isot. 101, 83 (2015)
- [21] E.G. Androulakaki et al., J. Environ. Radioact. 164, 253 (2016)
- [22] C. Tsabaris et al., HNPS Adv. Nucl. Phys., 29, 137 (2023)
- [23] The EGSnrc Code System: Monte Carlo Simulation of Electron and Photon Transport. I. Kawrakow, E. Mainegra-Hing, D.W.O. Rogers, F. Tessier, B.R.B. Walters. NRCC (2015)